A Combined Application of $\mathcal{H}_\infty$ Loop Shaping and μ-Synthesis to Control High-Speed Flywheels

Alexander Lanzon and Panagiotis Tsiotras

***Abstract*—The development of robust controllers for high-speed flywheel rotors supported on active magnetic bearings (AMBs) has been extensively studied over the past decade. Such flywheels can be used as energy momentum wheels (EMWs) onboard spacecraft, and pose a challenging control problem due to their high flexibility, nontrivial parametric uncertainty, and rotor-speed dependence. A combined $\mathcal{H}_\infty$ loop shaping and μ-synthesis approach is used in this paper to design controllers for EMWs supported on AMBs. This combination between these two well-established control methodologies is novel to the design of robust controllers for such systems. $\mathcal{H}_\infty$ loop shaping guarantees (through the specification of loop-shaping weights) closed-loop performance and robustness to generic unstructured coprime factor uncertainty, whereas robustness to highly directional parametric uncertainty is incorporated through a μ-synthesis design. Furthermore, in order to reduce the computational complexity of the control design and the order of the synthesized controllers, a method is proposed in this paper to reduce the number of states that depend on the rotor speed. The proposed methodology is demonstrated through numerical simulations and experimental results.**

***Index Terms*—Active magnetic bearings (AMBs), energy momentum wheels (EMWs), highly flexible systems, $\mathcal{H}_\infty$ loop shaping, robust control, μ-synthesis.**

I. Introduction

An ENERGY momentum wheel (EMW) is a flywheel that combines the functions of energy storage and momentum management into a single component. The successful application of EMWs to satellite systems, in particular, holds the promise of significantly reducing a satellite's mass and cost when contrasted with traditional satellite subsystem architectures that separate the energy storage and momentum management functions [2]–[5]. Active magnetic bearing (AMB) technology is crucial for efficient EMW operation due to the several advantages offered by AMBs, which include operation at very high speeds, no lubrication requirement, no wear, and low-power losses. In addition, spacecraft specifications often require stringent pointing requirements, as well as a vibration-free environment for onboard experiments. Imbalances and resonant modes in EMWs can create inertia forces which, when interacting with the stator, transmit unwanted vibration onto the spacecraft structure. This can be avoided with the use of AMBs coupled with an online controller that rejects undesirable vibrations [6], [7]. The successful development of an effective magnetic bearing controller is, thus, a critical technology for the use of EMWs in satellites.

Since most modern control design algorithms are model-based [8]–[12], developing an accurate mathematical model for the physical plant is a necessary and important first step prior to controller synthesis. The achievable performance of a controller depends not only on the control design algorithm but also on the accuracy of the mathematical model used for the plant [13]. A flexible rotor/magnetic bearing system, such as an EMW at high rotational speed, has time-varying and nonlinear characteristics that cannot be captured solely by a single linear time-invariant (LTI) model [14]–[16]. The splitting of the rotor mode shapes due to the gyroscopics, for example, have to be modeled via a parameter-dependent model, and the uncertainty in the rotor natural frequencies has to be adequately captured by highly directional parametric uncertainty. Hence, EMWs pose a challenging problem for most controller design techniques.

Conventional control methodologies for flywheels supported on AMBs typically assume a single LTI plant [17]–[19]. This is a reasonable assumption if the speed of the rotor remains constant. If, on the other hand, the speed of the rotor ranges over a wide spectrum of operating speeds (even if it varies very slowly)—as is the case for EMWs—the single LTI model assumption is no longer valid. This is because the system matrix of these plants is a function of the rotor speed and the plant dynamics change considerably with the rotor speed due to gyroscopic effects [15], [17], [20]. Consequently, conventional control algorithms, which do not give due consideration to the parameter-dependent nature of the plant, and instead treat speed-dependent changes in the dynamics as uncertainty, cannot achieve the desired performance when the system operates over a wide range of rotor speeds.

The greatest difficulty in designing controllers with good robust performance margins for EMWs operating at high rotor speeds is the highly resonant nature of the flexible modes. The proximity of the poles and zeros of such plants to the imaginary axis imposes fundamental limitations on the achievable performance [12], [21]. Together with the parameter-varying nature of the plant and the strict disturbance rejection specifications, these characteristics make ad hoc or trial-and-error designs for EMW/AMB systems inadequate.

In this paper, we model an EMW via a parameter-dependent nominal linear model, where the parameter is the rotor speed. In contrast to other robust techniques for EMWs proposed in

Manuscript received April 1, 2004. Manuscript received in final form January 20, 2005. Recommended by Associate Editor C. Knospe. This work was supported in part by the National Science Foundation under Award CMS-9996120, in part by the Air Force Office of Scientific Research under Award F49620-00-1-0374, in part by the Australian Research Council under Discovery-Projects Grant DP0342683, in part by National Information and Communication Technologies (ICT) Australia Ltd., which is funded through the Australian Government's Backing Australia's Ability Initiative, in part through the Australian Research Council.

A. Lanzon is with the Research School of Information Sciences and Engineering, The Australian National University, Canberra ACT 0200, Australia and also with National ICT Australia Ltd., Canberra ACT 2601, Australia.

P. Tsiotras is with the School of Aerospace Engineering, Georgia Institute of Technology, Atlanta, GA 30332-0150 USA (e-mail: p.tsiotras@ae.gatech.edu).

Digital Object Identifier 10.1109/TCST.2005.847344

1063-6536/$20.00 © 2005 IEEE

[17]–[19], this parameter-dependent model allows one to capture explicitly the changes of the dynamics due to the change or the rotor speed in the *nominal* plant, instead of treating them solely as unmodeled dynamics [22]. In addition, the highly directional uncertainty in the rotor natural frequencies is captured via parametric uncertainty; generic unmodeled dynamics is captured via unstructured coprime factor uncertainty. Assuming that the rotor speed varies slowly (i.e., the parameter in the model is quasi-static), we can neglect the effects of the rotor acceleration and, thus, restrict our designs on controllers that depend statically on the rotor speed. This assumption is certainly true for most EMW applications, where the rotor speed variation is much slower than the time-constant of the remaining system dynamics, and it simplifies the ensuing formulas.

We propose a combined application of $\mathcal{H}_\infty$ loop shaping and μ-synthesis to design robust controllers for EMW systems supported on AMBs. Although $\mathcal{H}_\infty$ loop shaping and μ-synthesis have been applied separately in the literature to control AMBs [17]–[20], the proposed combination of these two well-established control methodologies is novel to the design of robust controllers for AMB/EMW systems. Specifically, prior related designs for AMBs in [17]–[19] do not explicitly account for large variations in the speed of the rotor and, hence, they may not be suitable for EMW applications, where the speed of the wheel is expected to vary from 0 to 60 000 r/min or more [23]. Treating gyroscopics as purely unmodeled dynamics [17] will lead to conservative results. Gyroscopics are best captured within a gain-scheduling or linear parameter-varying (LPV) framework for the nominal plant. Reference [20] uses gain-scheduling to capture rotational variations, but the approach does not guard against parametric uncertainty and therefore it cannot capture discrepancies in the natural frequencies of the resonant modes. The importance of parametric uncertainty (other than gyroscopics) is recognized in [19] and [22] and treated using μ-synthesis. The latter reference does not deal with speed rotation variations therefore the approach is not directly applicable to EMW systems. In [22], both structured and unstructured uncertainty is included, but the effect of gyroscopics is again treated as an uncertainty. In [14], the authors also use μ-synthesis for the EMW/AMB problem, but they treat the rotor speed as an arbitrarily fast time-varying parametric uncertainty. Hence, the associated D-scales in the μ-synthesis procedure are constant as opposed to dynamic. Moreover, as in [17] and [22] the rotor speed is treated as an uncertainty, hence, the final design is an unnecessarily conservative robust LTI controller. None of the previous references (with the exception of [20]) recognizes the benefits of treating the rotor speed as a *known/measurable* time-varying parameter as opposed to an uncertainty. Parameter-variations due to the rotor speed have also been addressed in [15] and [16] in a nonconservative manner using gain-scheduling, but again these designs do not go far enough to be practical, since they do not capture directly parametric uncertainty in the flexible modes.

In this paper we integrate $\mathcal{H}_\infty$ loop shaping and μ-synthesis (with the added benefit of the potential for a gain-scheduling implementation), and propose a control design that is tailored to EMW/AMB applications. By combining $\mathcal{H}_\infty$ loop shaping and μ-synthesis we achieve the following objectives: 1) $\mathcal{H}_\infty$ loop shaping allows one to specify performance requirements through loop-shaping weights. Furthermore, it adds robustness to generic unstructured coprime factor uncertainty (which captures generic unmodeled dynamics such as substructure dynamics or higher order dynamics); 2) μ-synthesis guards against highly directional uncertainty in the rotor natural frequencies. Note that since even small mismatches in the natural frequencies of the vibrational modes can induce large unstructured uncertainty representations (whether it is additive, multiplicative or coprime factor errors is irrelevant [24]), it is of crucial importance to capture this type of uncertainty directly as highly directional parametric uncertainty [25].

It is noted that since the rotor speed parameter dependence of the nominal model is treated as a quasi-static uncertainty in the overall μ-synthesis design, the resulting controller will be robust to a wide range of rotor speeds. In the standard D–K iterative procedure, which will be used to solve the posed μ-synthesis problem, one typically associates a full-block dynamic D-scale with each repeated uncertainty block (in this case, the rotor speed dependence which was extracted as a quasi-static uncertainty). In order to reduce the computational complexity of the control design and the order of the synthesized controllers, we, therefore, also propose a method to reduce the number of states that depend on the rotor speed. Finally, we show how a gain-scheduled, robust controller emerges naturally from the proposed framework without extra effort.

II. Plant Model for a Typical EMW System Supported on AMBs

A. Nominal Plant Model

Typically, a nominal plant model for an EMW system supported on AMBs can be described by [15]

$$\begin{aligned} \dot{x} &= (A_o + \rho A_g)x + B_o u \\ y &= C_o x \end{aligned} \tag{1}$$

where ρ is the rotor spin speed, u is the vector of control inputs and y is the vector of measured displacements. The plant dynamics of such a system posses several features that make the control problem challenging from both a theoretical and an implementation stand-point. This is because typically such plants:

1) are unstable and nonminimum phase;
2) have nonnegligible time-delay;
3) are highly flexible with several flexible modes inside the desired closed-loop bandwidth;
4) have an LPV dependence on the rotor spin speed ρ;
5) have significant uncertainty on the natural frequencies of the flexible modes;
6) have significant unmodeled substructure dynamics.

These features, together with the required stringent performance specifications in terms of stability, robustness to unmodeled dynamics and uncertain parameters, and disturbance rejection over a wide frequency range, demand advanced control algorithms which are capable of handling these difficulties in a nonconservative and systematic way.

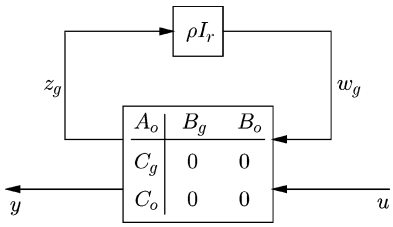

Fig. 1. Nominal plant with parameter ρ pulled-up in an LFT setup.

Properties 1), 2), and 3) listed previously will be handled via optimal controller design strategies ($\mathcal{H}_\infty$ control in this paper). Property 4) relates to the parameter dependence of the plant. As stated in the introduction, this parameter dependence on the rotor spin speed can be assumed quasi-static for EMW applications, although ρ must be allowed to vary over a wide range of spin speeds. Robustness to this kind of variation in the plant model will be ensured by "pulling out" this parameter dependence as quasi-static uncertainty and design a controller that is robust to this variation in ρ. Alternatively, variations in the parameter ρ can be addressed via gain-scheduled LPV design [15], [20], [26]; see also the discussion in the following. Property 5) relates to uncertainty on the natural frequency of the resonant modes. Again, as indicated in the introduction, if we use unstructured uncertainty (additive, multiplicative, coprime factor or otherwise) to capture mismatches in the natural frequencies of the flexible modes, we may end up with unstructured uncertainties of very large size [24]. Consequently, to reduce conservativeness in the design, it is better to capture this type of uncertainty directly as a highly directional parametric uncertainty. Finally, Property 6) relates to generic unmodeled dynamics. We choose to capture this via coprime factor uncertainty in an $\mathcal{H}_\infty$ loop-shaping framework. The reader is referred to [12] for extensive discussions why coprime factor uncertainty is the most generic form of unstructured uncertainty.

Notice that the nominal plant in (1) is not an LTI but rather an LPV system due to the dependence of the system matrix on the rotor speed ρ. These gyroscopic variations arise only in the modeling of the flexible rotor dynamics and not in other parts of the system, thus the matrix A_g is typically rank deficient. Consequently, it is possible to decompose A_g into $A_g = B_g C_g$ where the number of columns of B_g and the number of rows of C_g are equal to the rank of A_g [27]. Using this decomposition, the parameter ρ may be pulled-out in an LFT setup as shown in Fig. 1, where r denotes the rank of A_g. This LFT formulation has several advantages. First, it allows one to make connections with standard robust control ideas. Second, it makes the parameter ρ available to the controller for a parameter-varying design—see the discussion in Section III. Finally, it allows the reduction in the number of states that depend on ρ, thus, speeding up both the process of control design as well as the controller implementation. This is explained in Section II-C.

B. Plant Model With Uncertainty on Modal Frequencies

In order for a controller to perform well on a physical plant, the uncertainty characterization for the nominal plant model must be such that it captures the dynamics of the true plant. The predominant source of uncertainty in EMW systems is due to the lack of knowledge in the natural frequencies of the vibrational modes. Since even small mismatches in the natural frequencies of vibrational modes can induce large unstructured uncertainty representations (additive, multiplicative or coprime factor errors [24]), it is crucial to capture this type of uncertainty directly as highly directional parametric uncertainty [25].

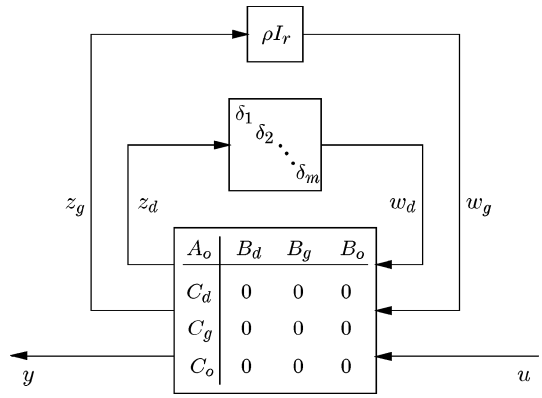

Fig. 2. Perturbed plant with parametric uncertainty $\delta_1, \ldots, \delta_m \in \mathbb{R}$.

Toward this end, let A_o be the system matrix in the nominal plant model. Then, A_o can be transformed to a real modal representation $\tilde{A} = T A_o T^{-1}$ through a similarity transformation matrix T. Then the 2×2 block corresponding to the ith vibrational mode on the main diagonal of $\tilde{A}$ is of the form

$$\tilde{A}_i = \begin{bmatrix} 0 & 1 \\ -[\omega_i(1+\delta_i)]^2 & -2\xi_i[\omega_i(1+\delta_i)] \end{bmatrix}$$

where ξ_i is the modal damping of the ith mode, which is assumed to be known, and ω_i is the natural frequency of the ith mode with relative multiplicative uncertainty δ_i. Linearizing the term $[\omega_i(1+\delta_i)]^2$ for small uncertainties δ_i gives $\omega_i^2 + 2\omega_i^2\delta_i$ and, hence, $\tilde{A}_i$ can be rewritten as

$$\tilde{A}_i = \begin{bmatrix} 0 & 1 \\ -\omega_i^2 & -2\xi_i\omega_i \end{bmatrix} + \begin{bmatrix} 0 \\ 1 \end{bmatrix} \delta_i \begin{bmatrix} -2\omega_i^2 & -2\xi_i\omega_i \end{bmatrix}.$$

Thus, $\tilde{A}_i$ can be represented in an LFT setup with the input and output vectors

$$\tilde{B}_i = \begin{bmatrix} 0 \\ 1 \end{bmatrix} \quad \text{and} \quad \tilde{C}_i = \begin{bmatrix} -2\omega_i^2 & -2\xi_i\omega_i \end{bmatrix}$$

and a single real uncertainty $\delta_i \in \mathbb{R}$. In order to keep the numerical condition of the original plant model and the same state representation, the plant model is not kept to the modal coordinates. Instead, the input and output uncertainty matrices $\tilde{B}$ and $\tilde{C}$, assembled from the vectors $\tilde{B}_i$ and $\tilde{C}_i$, are transformed back to the original coordinates: $C_d = \tilde{C}T$ and $B_d = T^{-1}\tilde{B}$. The numeric conditioning of these input and output matrices B_d and C_d is further improved by scaling the rows and columns of C_d and B_d, respectively, to have equal 2-norms. The perturbed plant model so achieved is depicted in Fig. 2.

C. Reduction of Number of Plant States That Depend on ρ

Consider the task of synthesizing a controller in the μ-synthesis framework for a plant of the form of Fig. 2 with ρI_r

treated as a (quasistatic) uncertainty using the standard D–K iteration [28]. Corresponding to the uncertainty block ρI_r, there will be a full-block dynamic D-scale of dimension $r \times r$. In a typical D–K iterative procedure, the D-scales are first computed pointwise in frequency and then the resulting frequency data for each element is fitted by a transfer function in order to construct a rational D-scale that can be used for a subsequent controller synthesis. If r is not a small number, this procedure can easily result in a rational D-scale that has very high order. Such a high-order D-scale will then, in turn, result in a high-order synthesized controller, which is perhaps unsuitable for direct implementation. Clearly, there is great benefit both computationally and numerically if r can be reduced with minor compromise in the modeling accuracy and achieved performance, as this will result in lower order controller synthesis. The basis of such a reduction in the number of states r that depend on the spin speed ρ will be in this paper the ν-gap metric [29].

Toward this end, let the choices of B_g and C_g in the decomposition of $A_g = B_g C_g$ be as follows:

$$B_g := U\begin{bmatrix}\Theta\\ 0\end{bmatrix} \quad \text{and} \quad C_g := [I_r \quad 0]U^T$$

where $A_g = U\begin{bmatrix}\Theta & 0\\ 0 & 0\end{bmatrix}U^T$ is a Real Schur Decomposition of A_g with U satisfying $UU^T = U^TU = I$ and

$$\Theta = \operatorname{diag}\left(\begin{bmatrix}0 & \sigma_1\\ -\sigma_1 & 0\end{bmatrix}, \begin{bmatrix}0 & \sigma_2\\ -\sigma_2 & 0\end{bmatrix}, \cdots, \begin{bmatrix}0 & \sigma_{\frac{r}{2}}\\ -\sigma_{\frac{r}{2}} & 0\end{bmatrix}\right)$$

with $\sigma_1 \geq \sigma_2 \geq \cdots \geq \sigma_{r/2} > 0$. Note that Θ takes this special form because A_g is skew-symmetric (i.e., $A_g = -A_g^T$) for EMW systems [30]. Then, we can define a new perturbed plant model $\bar{P}_q$, with $\hat{B}_g = B_g\begin{bmatrix}I_q\\ 0\end{bmatrix}$ replacing B_g and $\hat{C}_g = [I_q \ 0]C_g$ replacing C_g. The only difference between this new perturbed plant model $\bar{P}_q$ and the original perturbed plant model $\bar{P}$ of Fig. 2 is the number of states that depend on the spin speed ρ. Note that this process of constructing $\bar{P}_q$ effectively truncates the smallest singular values of A_g.

A fundamental property of the ν-gap metric is captured by the following result [29]: "Given any two plants P_1, P_2 of same input–output dimensions and a controller C of compatible dimensions

$$b(P_2, C) \geq b(P_1, C) - \delta_\nu(P_1, P_2)." \tag{2}$$

The reader is referred to [29] for appropriate definitions of the ν-gap metric $\delta_\nu(P_1, P_2)$ and the generalized robust stability margins $b(P_i, C)$ and $b_{\text{opt}}(P_i)$. The previous result implies that if a controller C performs sufficiently well with P_1 (in terms of $b(P_1, C)$ being sufficiently large), and if the ν-gap between P_1 and P_2 is sufficiently small, then C is guaranteed to achieve a certain level of performance with P_2. Hence, the ν-gap metric gives us a bound on the maximum allowable degradation in performance and robustness when plant P_1 is replaced by plant P_2 in a control systems design.

This result, thus, turns out to be very useful in proposing a method for reducing the number of states that depend on the spin speed ρ, as it provides us with a guaranteed bound on the maximum allowable degradation in performance and robustness when using the reduced plant instead of the original plant. The following procedure can, hence, be used to determine the smallest value of q such that the systems $\bar{P}_q$ and $\bar{P}$ are close in a *feedback sense*.

1) Let $q = r$ and evaluate $\inf_{\delta_i} b_{\text{opt}}(W_2\bar{P}W_1)$ at every ρ in the operating envelope.
2) Evaluate $\sup_{\delta_i} \delta_\nu(W_2\bar{P}W_1, W_2\bar{P}_{q-1}W_1)$ at every ρ in the operating envelope.
3) If $\sup_{\delta_i} \delta_\nu(W_2\bar{P}W_1, W_2\bar{P}_{q-1}W_1) \ll \inf_{\delta_i} b_{\text{opt}}(W_2\bar{P}W_1)$ at every ρ in the operating envelope, then let $q = q - 1$ and go back to Step 2). Otherwise EXIT.

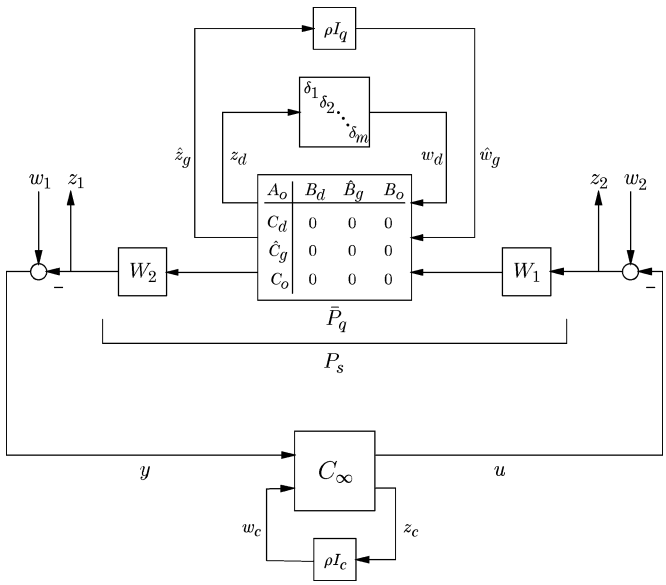

Fig. 3. Block diagram for $\mathcal{H}_\infty$ loop-shaping framework. Since the rotor speed ρ is known, it can be used by the controller in a gain-scheduling framework. By setting $c = 0$ one obtains an LTI controller.

The weights W_1 and W_2 are loop-shaping weights. They will be discussed in detail in Section III-A. At this stage, it should suffice to think of these weights as objects that somehow capture the robust performance requirements.

Clearly, other model reduction techniques could also be used [31]. However, unlike most other model reduction techniques, the procedure outlined previously gives guarantees on the maximum performance degradation in the generalized robust stability margin and, hence, the maximum performance degradation in an $\mathcal{H}_\infty$ loop-shaping design in the following sense: The generalized robust stability margin $b(W_2\bar{P}_qW_1, \mathcal{F}_l(C_\infty, \rho I_c))$ is the reciprocal of the size (in an $\mathcal{H}_\infty$ sense) of the transfer function from $[w_1^T \ w_2^T]^T$ to $[z_1^T \ z_2^T]^T$ in Fig. 3. Consequently, via a small gain argument, the system of Fig. 3 will remain well-posed and internally stable for all full block uncertainties connected from $[z_1^T \ z_2^T]^T$ to $[w_1^T \ w_2^T]^T$ of size (in an $\mathcal{H}_\infty$ sense) strictly less than $b(W_2\bar{P}_qW_1, \mathcal{F}_l(C_\infty, \rho I_c))$ (see also Fig. 4 for a normalized version of this full block uncertainty Δ). Now, the maximum performance degradation $\sup_{\delta_i} \delta_\nu(W_2\bar{P}W_1, W_2\bar{P}_{q-1}W_1)$ given by the previous procedure is exactly the degradation in $b(W_2\bar{P}_qW_1, \mathcal{F}_l(C_\infty, \rho I_c))$ [via inequality (2)] and, hence,

exactly the degradation in the maximum allowable size of the full block uncertainty (which when normalized gives Δ in Fig. 4). Note that this entire reasoning is closely related to a skewed-μ degradation in performance [32], wherein only the performance uncertainty block degrades but not the physical uncertainty blocks.

III. Control Problem Formulation

In this section, the control problem of interest is formulated. Given a plant model for an EMW system with an uncertainty characterization as illustrated in Fig. 2, the control problem is cast into an $\mathcal{H}_\infty$ loop-shaping design problem as depicted in Fig. 3. On comparing Fig. 3 with a standard LTI $\mathcal{H}_\infty$ loop-shaping block diagram, two differences emerge: (a) the plant model P in Fig. 3 is a function of the parameter ρ and has parametric uncertainty on the natural frequencies of the vibrational modes, and (b) the controller is a function of the parameter ρ. It should be clear from Fig. 3 that setting $c = 0$ gives an LTI controller (independent of the parameter ρ), whereas setting $c > 0$ gives a gain-scheduled controller that is a function of ρ.

Specifically, since the synthesized C_∞ will be strictly proper (for a suboptimal $\mathcal{H}_\infty$ loop-shaping design), the proposed scheme can be used to yield a gain-scheduled controller $C(\rho)$ of the form

$$\begin{aligned}\dot{x}_k &= \left(A_{k_o} + \rho A_{k_g}\right) x_k + B_{k_o} y \\ u &= C_{k_o} x_k\end{aligned}$$

where $\operatorname{rank}(A_{k_g}) = c$. This gain-scheduled controller would have the same form as that of the parameter-varying plant. Furthermore, since the dimension of the uncertainty block that depends on the parameter ρ is q in the plant and c in the controller, there is no reason to choose c greater than q.

A. Selection of Loop-Shaping Weights

The loop-shaping weights W_1 and W_2 in Fig. 3 are designed in two stages.

In the first stage, the desired loop shape is determined. This usually involves translating time-response requirements and closed-loop performance specifications into the frequency domain. To do this, engineers largely rely on their intuition and their past experience with loop-shaping concepts. Roughly speaking the loop gain should be large at low frequencies to achieve good performance, small at high frequencies to guard against unmodeled dynamics and noise, and have a gentle slope around crossover to maintain stability [24], [33], [34]. In the second stage, the designer selects loop-shaping weights W_1 and W_2 so that P_s has the desired loop shape. Diagonal weights are often adequate to achieve the desired loop shape [35]. However, some design examples have shown that diagonal weights do not work well for plants with strong crosscoupling between the channels. In such cases, nondiagonal weights are necessary which are of course more difficult to design. Selecting loop-shaping weights that are independent of ρ means that the resulting controller will be LTI when $c = 0$ since the controller which will be implemented on the true plant will be $C = W_1 C_\infty W_2$. On the other hand, ρ-dependent weights will result in a parameter-dependent controller (even when $c = 0$) since the controller implemented on the plant will be $C(\rho) = W_1(\rho)\mathcal{F}_l(C_\infty, \rho I_c)W_2(\rho)$.

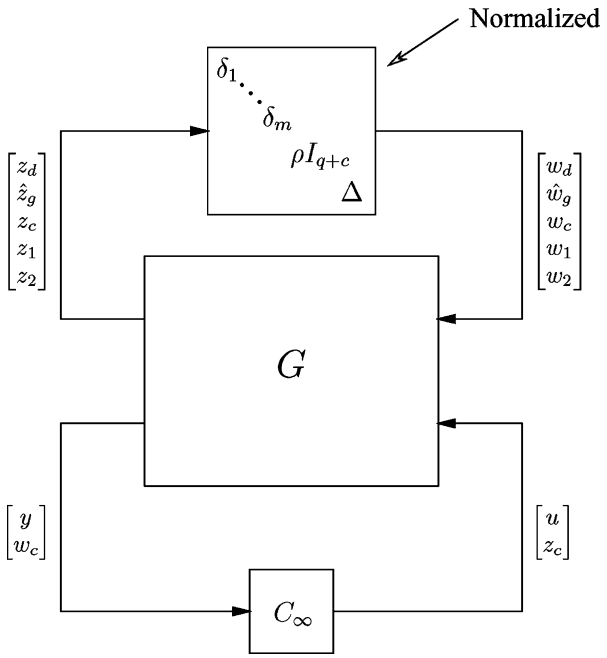

Fig. 4. LFT interconnection for C_∞ synthesis.

In order to synthesize C_∞, the block diagram of Fig. 3 is redrawn into the LFT configuration of Fig. 4. Here, G is the generalized plant and consists of all known or specified transfer functions in the feedback interconnection, C_∞ is the LTI system to be synthesized, and $\operatorname{diag}[\delta_1, \ldots, \delta_m, \rho I_{q+c}, \Delta]$ is the structured and *normalized* uncertainty block in the system. Note that if $c = 0$, the signals w_c, z_c and the corresponding subblocks in C_∞, G and the uncertainty block disappear from the formulation. Since the structured uncertainty block is normalized to have size less than or equal to unity, a necessary and sufficient condition for robust performance of this interconnection is that

$$\sup_{\omega \in \mathbb{R}} \mu_{\mathbf{\Delta}_{\mathrm{TOT}}} \left[\mathcal{F}_l\left(G(j\omega), C_\infty(j\omega)\right)\right] < 1$$

where $\mathbf{\Delta}_{\mathrm{TOT}}$ specifies the structure of the uncertainty block. The problem of synthesizing C_∞, thus, reduces to a standard μ-synthesis problem which can be solved through a D–K iterative procedure.

In the remaining sections of the paper, we will provide the details of the experimental validation of a robust LTI controller using the proposed approach. Therefore, we will assume that $c = 0$. This restriction to an LTI design was merely chosen for consistency with the available experimental data, since the test rig used to conduct the experiments did not allow the implementation of gain-scheduled controllers at the time. It is reminded however that the proposed design is more general and a gain-scheduled version of this controller may be obtained simply by defining $c > 0$ in the previous formulae.

IV. Experimental Rig Description and Modelling

The previous design algorithm was experimentally tested on a test rig constructed to include most (if not all) important features of an EMW device [22], namely, high flexibility, large gyro-

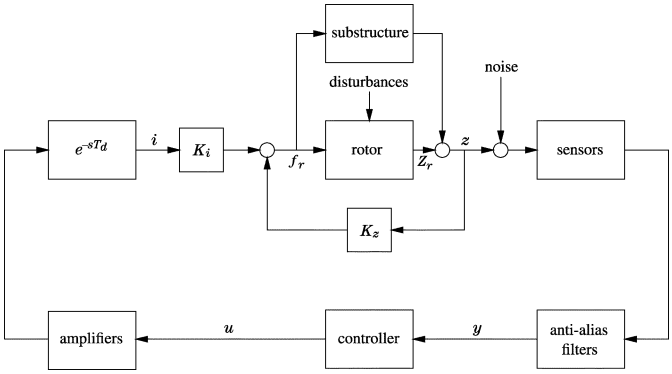

Fig. 5. Block diagram for closed-loop system of the test rig used for the experiments.

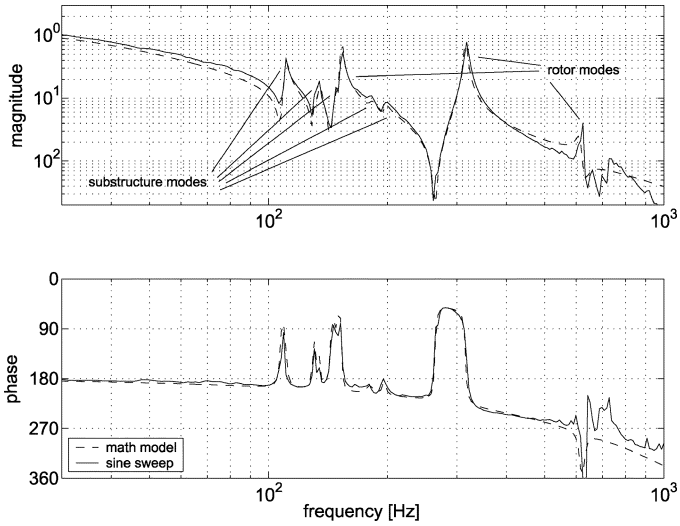

Fig. 6. Frequency response of test rig. Comparison between rotor mathematical model and experiment.

scopics, etc. The test rig consists of a shaft in an overhanging configuration and it has a maximum speed of approximately 15 000 r/min. A thrust magnetic bearing located at the top of the shaft, supports the rotor vertically. Two sets of radial magnetic bearings are located in the middle of the rotor shaft, with one set labeled as higher bearing and the other set labeled as lower bearing. An additional set of mechanical bearings, located next to the radial magnetic bearings, are used as backup bearings. Eddy-current displacement probes are used to pick up the displacement signals of the rotor. The design also completely integrates the motor with the rotor shaft. A gyroscopic disk, simulating the gyroscopic effects of a flywheel, is located at the bottom of the shaft.

Besides all the mechanical parts just described, the system also consists of amplifiers for the actuators, sensors and anti-alias filters for digital control. Furthermore, interaction of this system with the surrounding structure is modeled by a substructure transfer function. The block diagram for the closed-loop system is shown in Fig. 5. In order to have effective model-based control designs, accurate mathematical models were developed for each component in the physical system and validated through extensive experimental testing.

Fig. 6 shows the transfer function of the model from the top y axis bearing actuator to the top y axis sensor. The figure shows the high fidelity of the model used for controller validation. The other transfer functions were similar. The reader is referred to [22] for a detailed description of the test rig used for the experiments including each subsystem's modeling procedure and assumptions.

A. Nominal Plant Model

A reduced order model was obtained for control design. This reduced order nominal model includes all the plant components in Fig. 5, has 44 states and can be described as in (1), where the control input u is the voltage command to the amplifiers, and the output vector y is the filtered voltage measurement of displacements (see Fig. 5). The matrix A_g that captures the gyroscopic dynamics is rank deficient, with rank $A_g = 10$.

The singular values of the nominal plant plotted against frequency at four different values of the parameter ρ are depicted in Fig. 7. These singular value plots clearly illustrate the level of flexibility and the nontrivial variation of the plant with the parameter ρ. Since the highest unstable pole is at 250 rad/s and the lowest unstable zero is at 5550 rad/s, it is desirable to set the closed-loop bandwidth between 250 rad/s and 5550 rad/s [24], [33], [34]. The closed-loop performance specifications in fact require a closed-loop bandwidth around 2000 rad/s, as there will be disturbances which need to be attenuated up to this frequency. Such a closed-loop bandwidth necessitates fast sampling rates for digital implementation of the controller. Consequently, the computation time allowed for calculating the control law is quite short. It, thus, becomes clear that the order of the synthesized controller should be kept as small as possible, and that any gain-scheduled controller must minimize the number of elements that are updated and/or depend on the rotor speed. The rank deficiency of A_g, along with the fact that the parameter ρ typically changes slowly for EMW applications should be exploited in order to reduce the online computations.

B. Reduction of Number of Plant States That Depend on ρ

As shown in Fig. 1, we can exploit the rank deficiency in matrix A_g to extract the spin speed ρ as "uncertainty." As explained earlier, since in a typical EMW application ρ varies very slowly when compared to the remaining system dynamics, ρI_r can be treated as a quasi-static uncertainty and, hence, in a D–K iterative procedure, a full-block rational D-scale of dimension $r \times r$ would need to be associated with it. Since rank $A_g = 10$ it follows that that a full-block rational D-scale with 100 elements need to be constructed from the frequency-by-frequency data. Such a high-order D-scale would result in a high-order controller design. This is clearly not desirable.

As explained in Section II-C, we can do significantly better by reducing the number of states in the plant that depend on the spin speed ρ. Following the procedure outlined in that section, and since experience suggests that $b_{\text{opt}}(W_2\bar{P}W_1) > 0.2$ is a good value in practice (see [34] for justification), we get $q = 8$ as the smallest value of q such that $\bar{P}_q$ and $\bar{P}$ are close in a feedback sense. This implies a reduction of two states (since $r = 10$) from the dependence on ρ. This yields considerable computational improvement as there are now 64 elements for the D-scale associated with ρI_q when compared to 100 elements

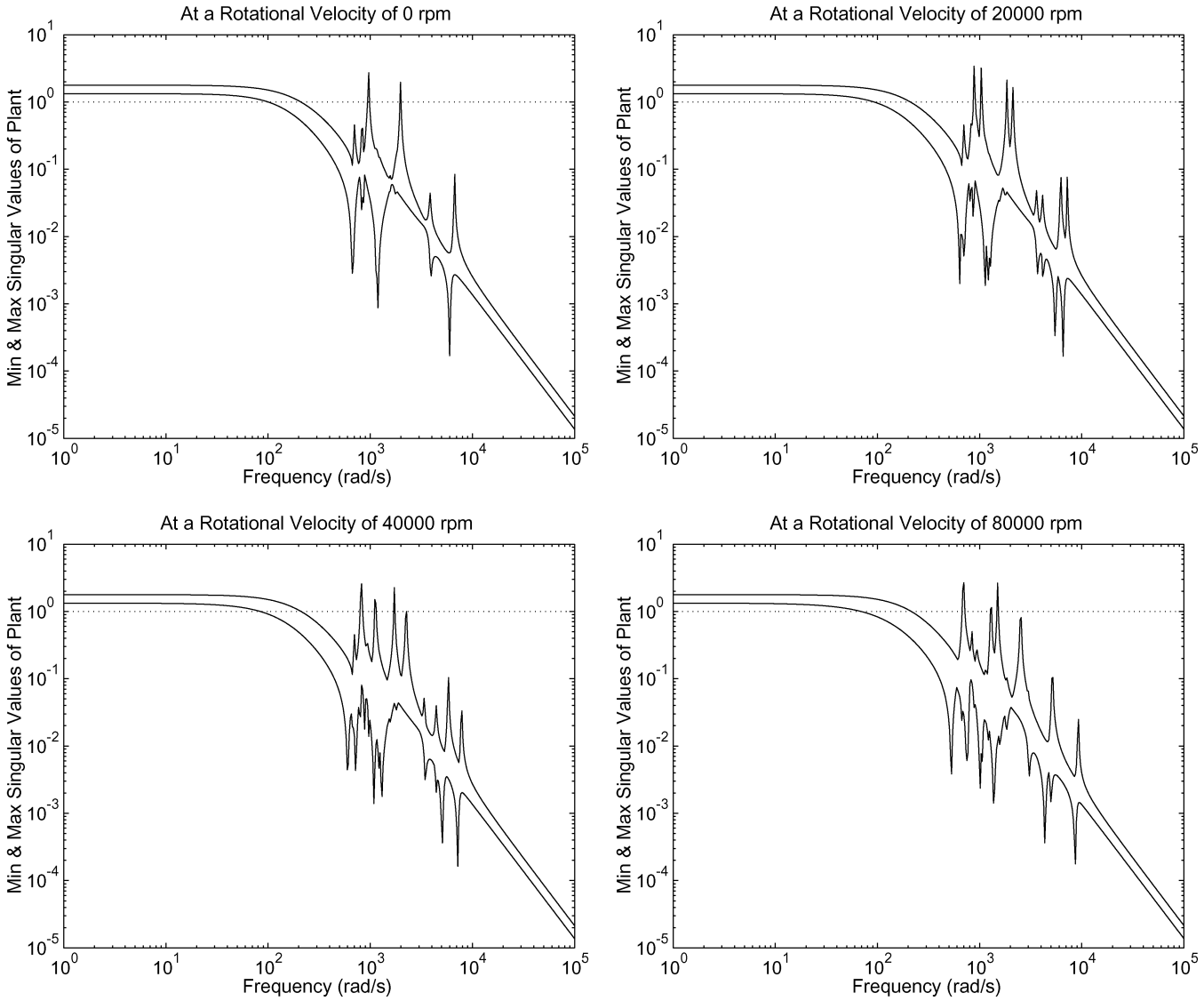

Fig. 7. Singular values of plant dynamics.

for the D-scale associated with ρI_r (i.e., a savings of 36% in fitting rational functions to pointwise-in-frequency data).

C. Plant Model With Uncertainty on Modal Frequencies

Since the modal frequencies for the test rig used in the experiments are not well known, an uncertain model had to be developed. This was done by extracting the modal information from the nominal plant model (1) and using the method outlined in Section II-B. We performed a number of sine sweeps on the experimental rig, each of which resulted in a slightly different reading for the natural frequencies of the resonant modes. On the basis of these experiments, we concluded that $\mathrm{a} \pm 6\%$ multiplicative uncertainty on the natural frequencies of the vibrational modes could be considered adequate coverage. Uncertainty in the mode shapes was accounted for by the coprime factor uncertainty description. Recall that the mode shapes are related to the zeros of the system which are characterized by one of the coprime factors of the plant [36] (the other one characterizing the poles).

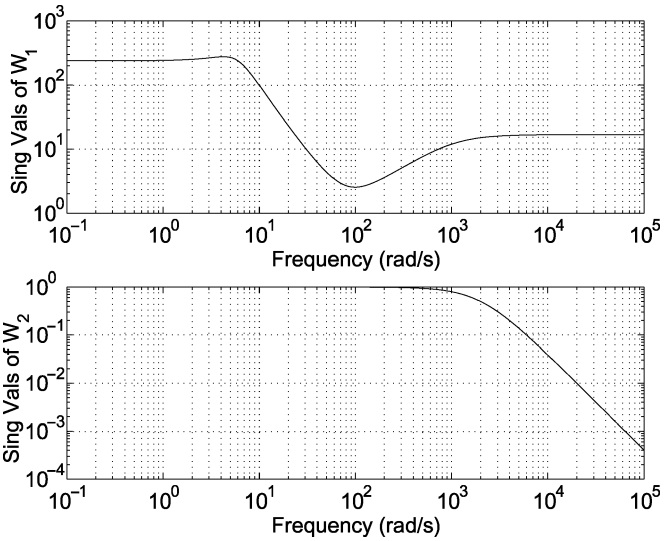

Fig. 8. Loop-shaping weights W_1 and W_2.

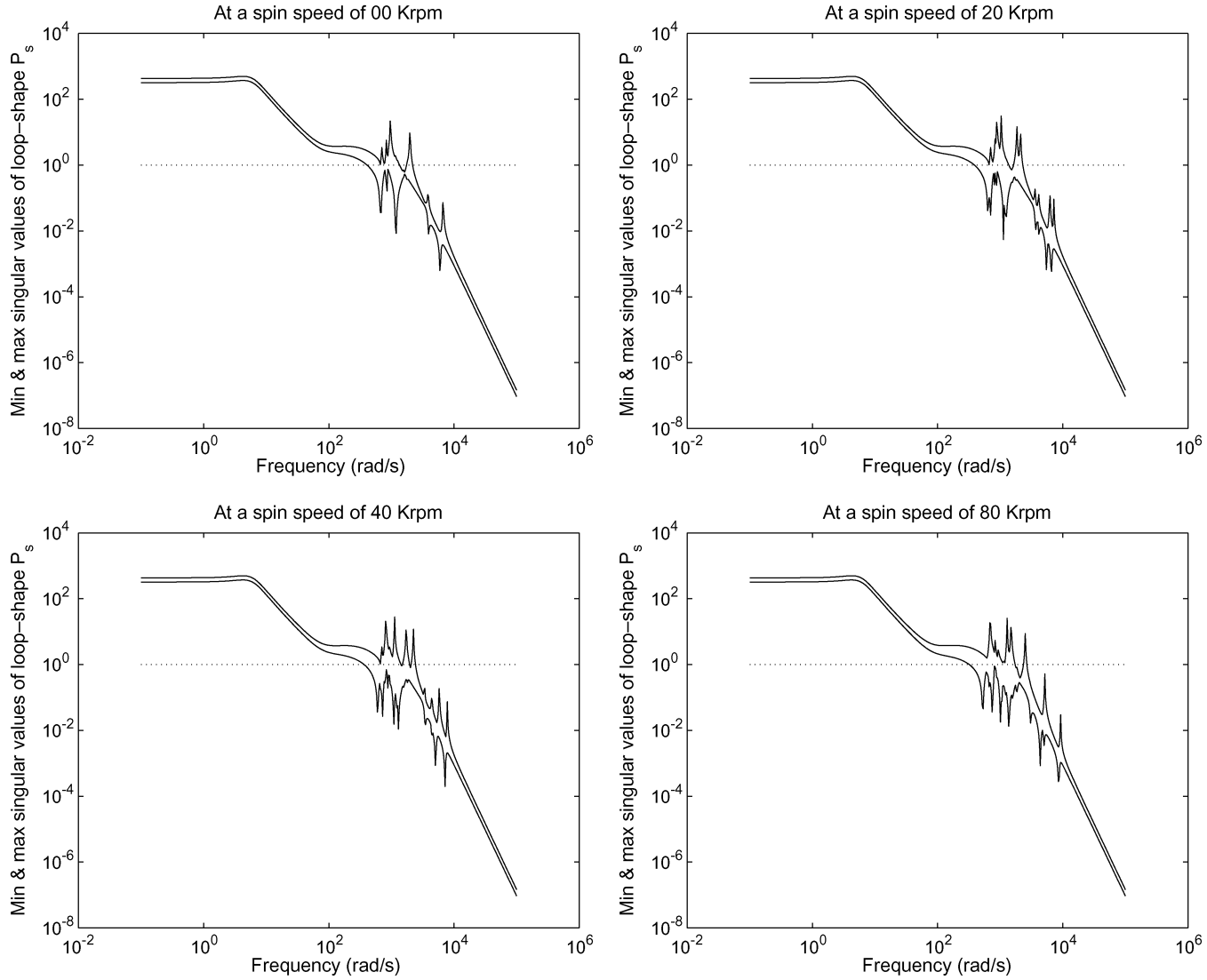

Fig. 9. Loop-shape plots for P_s at various rotor spin speeds.

V. Controller Synthesis and Simulation/Experimental Results

Performance specifications for this EMW test rig call for a sensitivity reduction of 100 times at low frequency (so that regulation errors are less than 1% at low frequency) and a complementary sensitivity, control effort, and sensor noise reduction of at least 40 dB/decade at high frequency (this reduction in the complementary sensitivity function is required to reduce the effects of high-frequency unmodeled dynamics due to interaction with the substructure). Also, as discussed earlier, a closed-loop bandwidth of approximately 2000 rad/s is desired since this will guarantee a regulation time constant of approximately 3 ms. These three specifications can be captured in the $\mathcal{H}_\infty$ loop-shaping framework by choosing the following loop-shaping weights:

$$W_1 = \frac{17(s^2+112s+6400)(s+80)}{(s^2+6s+36)(s+1000)} I_4$$

and

$$W_2 = \frac{2000^2}{(s+2000)^2} I_4$$

which are also depicted in Fig. 8.

In order to explain how these weights were designed, first note that W_2 is a low-pass filter with a gain of unity at low frequency and a rolloff rate of 40 dB/decade at high frequency after 2000 rad/s. This ensures that the desired rolloff rate is achieved after 2000 rad/s. Consequently, weight W_2 has no other purpose in this design besides ensuring this high-frequency rolloff rate. On the other hand, W_1 is chosen to have a gain greater than 100 at low frequency thereby ensuring that the required sensitivity reduction level is achieved at low frequency. Also, this gain reduces in the midfrequency region in order to secure a closed-loop bandwidth of approximately 2000 rad/s. Furthermore, we choose W_1 to also introduce some phase lead slightly before the desired closed-loop bandwidth so as to obtain decent stability margins. This qualitatively explains the shape of W_1. At high frequency, W_1 remains constant as the required rolloff rate is achieved via W_2. The weight W_1 was chosen to be third-order because we wanted to maintain the gain of W_1 above 100 up to at least 10 rad/s and then it was required for W_1 to go from 100 to almost a gain of 1 in one decade of frequency (from 10 rad/s to 100 rad/s). In a practical $\mathcal{H}_\infty$ loop-shaping design, diagonal weights are frequently sufficient to alter the singular values of the plant in such a way that specifications are met and

a decent robust stability margin is achieved [35]. For this experiment, as is usually the case in practice, diagonal weights did the job very well and, hence, there was no need of exploring the use of nondiagonal loop-shaping weights.

A plot of the resulting loop shape (after defining the previous parameter independent loop-shaping weights) at various rotor spin speeds is given in Fig. 9. It is clear from this figure that the designed loop-shaping weights achieve the desired rolloff rate, low-frequency gain and closed-loop bandwidth.

Now that the loop-shaping weights have been designed, we cast the closed-loop interconnection into the LFT framework of Fig. 4, where G is the generalized plant, C_∞ is the system we wish to synthesize and δ_i, ρI_{q+c} and Δ are uncertainties in the system. The bound on the size of these uncertainties has to be normalized (say to unity) before we can cast the problem of synthesizing the LTI system C_∞ as a standard μ-synthesis problem. That is:

"Find a stabilizing C_∞ such that $\sup_\omega \mu_{\mathbf{\Delta}_{\rm TOT}}[\mathcal{F}_l(G, C_\infty)(j\omega)] < 1$."

In order to perform this normalization, we have to first determine the bound on the size of each of these uncertainties δ_i, ρI_{q+c} and Δ. It was argued in Section IV-C that we need to consider 6% parametric uncertainty (i.e., $\|\delta_i\|_\infty \leq 0.06$) on the natural frequency of each of the vibrational modes in order to adequately capture imprecisions in the modeled natural frequencies. Also, standard $\mathcal{H}_\infty$ loop-shaping literature [37]–[39] argues that 20% unstructured uncertainty on the normalized coprime factors of the shaped plant (i.e., $\|\Delta\|_\infty \leq 0.20$) is adequate robustness to unmodeled dynamics since it corresponds to 3.5 dB of gain margin and 23° of phase margin [39] in a classical design. We also need to determine a bound on the size of the allowable parameter variations ρ in the quasi-static uncertainty ρI_{q+r}. A permissible parameter variation in ρ from 0 to 2000 r/min was determined (for the case $c = 0$) using a bisection search algorithm that checked the condition:

"Does there exist a stabilizing C_∞ such that $\sup_\omega \mu_{\mathbf{\Delta}_{\rm TOT}}[\mathcal{F}_l(G, C_\infty)(j\omega)] < 1$?"

at each value of the proposed bound on ρ given by this bisection search. Note that this idea is very similar to skewed-μ ideas [32] and related synthesis procedures [40]–[42].

An LTI controller was synthesized for the test rig by setting $c = 0$ in Figs. 3 and 4 using the approach outlined in the previous sections. The resulting overall μ-synthesis problem was solved via the standard D–K iterative procedure. The synthesized controller has 56 states and achieves robust performance in the face of the specified uncertainties discussed previously.

We note that even though one could use the D/G–K iterative procedure [43], [44] to solve a mixed real/complex μ-problem [45] (since δ_i and ρ are real), we deliberately chose to embed these real uncertainties into complex uncertainties, hence, needing only D-scales and no G-scales. This was done for reasons of computational ease, order of synthesized controllers, and for numerical reliability of the associated MATLAB functions.

Fig. 10 shows the singular value plots for the synthesized LTI system C_∞ and the controller $C = W_1 C_\infty W_2$ implemented on the plant P. It can be seen that the controller C has

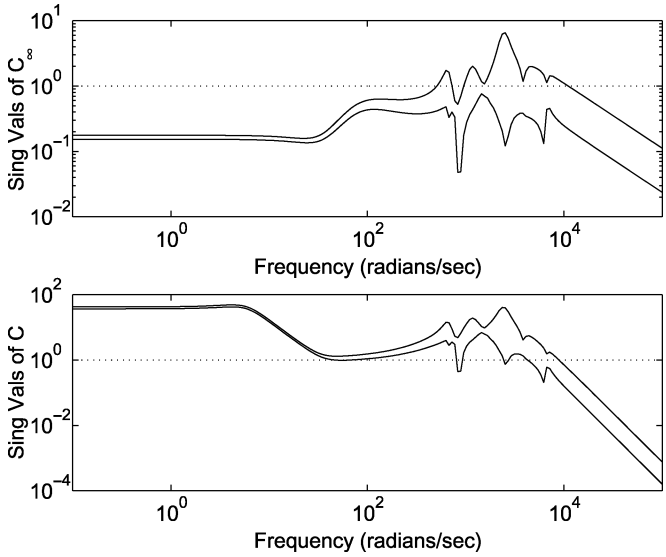

Fig. 10. Controller singular value plots.

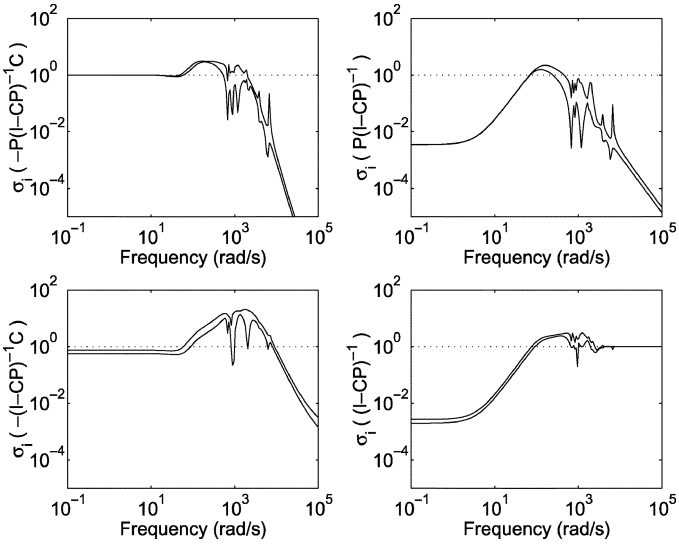

Fig. 11. Singular value plots for sensitivity, plant input disturbance rejection, control effort, and complementary sensitivity.

high gain at low frequency to achieve the desired sensitivity reduction and rolls off rapidly after 5000 rad/s to reduce the effects of spill-over dynamics. The complex dynamics of the controller around crossover are due to the vibrational modes in the plant, since lightly damped poles and zeros around crossover can be detrimental to stability if the controller does not adequately compensate for them.

A. Simulation and Experimental Results

This controller was tested both in simulations on the full-order plant model (i.e., the plant model of the experimental rig which was not model-reduced for controller synthesis), as well on the actual test rig described in the previous section. The simulations and experimental results from the test rig were very comparable. This was due to the high fidelity of the mathematical model used for the numerical simulations [22] and the realistic, nonconservative uncertainty description used for controller synthesis. Both in numerical simulations and the experiments the system retained stability and an adequate level of performance

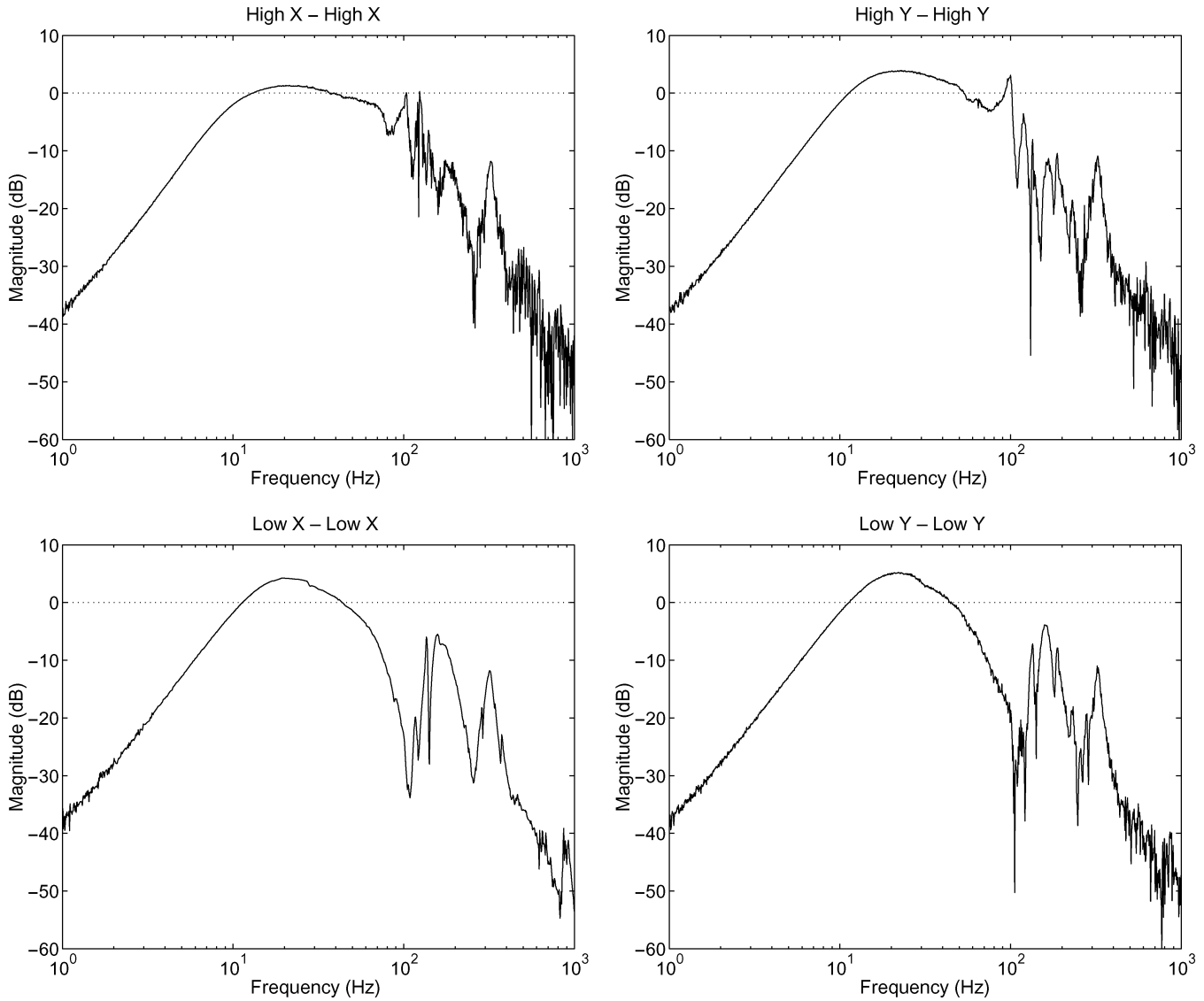

Fig. 12. Magnitude plots of $(I - PC)^{-1}P$ from experiments.

up to 15 000 r/min (just beyond the first two resonant modes[1]). Experimental data from the 0 r/min case are presented in the following.

The singular value plots (at 0 r/min) of the achieved sensitivity, complementary sensitivity, plant input disturbance rejection and control effort for this design are given in Fig. 11. These four transfer functions are important, as they fully describe the closed-loop behavior of a feedback interconnection (see [12], [24], and [37] for extensive discussion). From these figures, it can be seen that sensitivity reduction is obtained up to 100 rad/s and complementary sensitivity reduction is obtained beyond 2000 rad/s. The latter specifies the robustness to spill-over dynamics. Control effort is approximately equal to unity until 100 rad/s and decreases to zero beyond 10 000 rad/s. In the crossover frequency range, the control effort increases to 20 dB because the controller has to do sufficient work to compensate for the uncertain vibrational modes of the plant. The 20-dB gain of the control signal was sufficiently low to never saturate the actuators. Finally, the plant input disturbance rejection transfer function is small in the low- and high-frequency ranges and is approximately unity in the midfrequency range. This transfer function corresponds to the desirable closed-loop disturbance rejection properties.

The plant input disturbance rejection magnitude responses obtained during the experiments are given in Fig. 12. These transfer functions are important in this application because the expected disturbances in this application are mostly plant input disturbances. In fact, these disturbances are the most problematic in EMW systems due to the lightly damped nature of the plant. The plant input disturbance rejection time responses for a step disturbance of unit magnitude are shown in Fig. 13. Fig. 12 shows that plant input disturbance rejection transfer function reduction was achieved for all four channels until 10 Hz and beyond 200 Hz. Furthermore, the controller dealt with the resonant modes adequately around crossover since these transfer functions are not larger than 5 dB in the midfrequency range. This implies that the closed-loop system is able to attenuate distur-

[1]Numerical simulations against the high-fidelity model actually showed that a gain-scheduled version of this controller, i.e., $c = q$, achieves operation till 80 000 r/min.

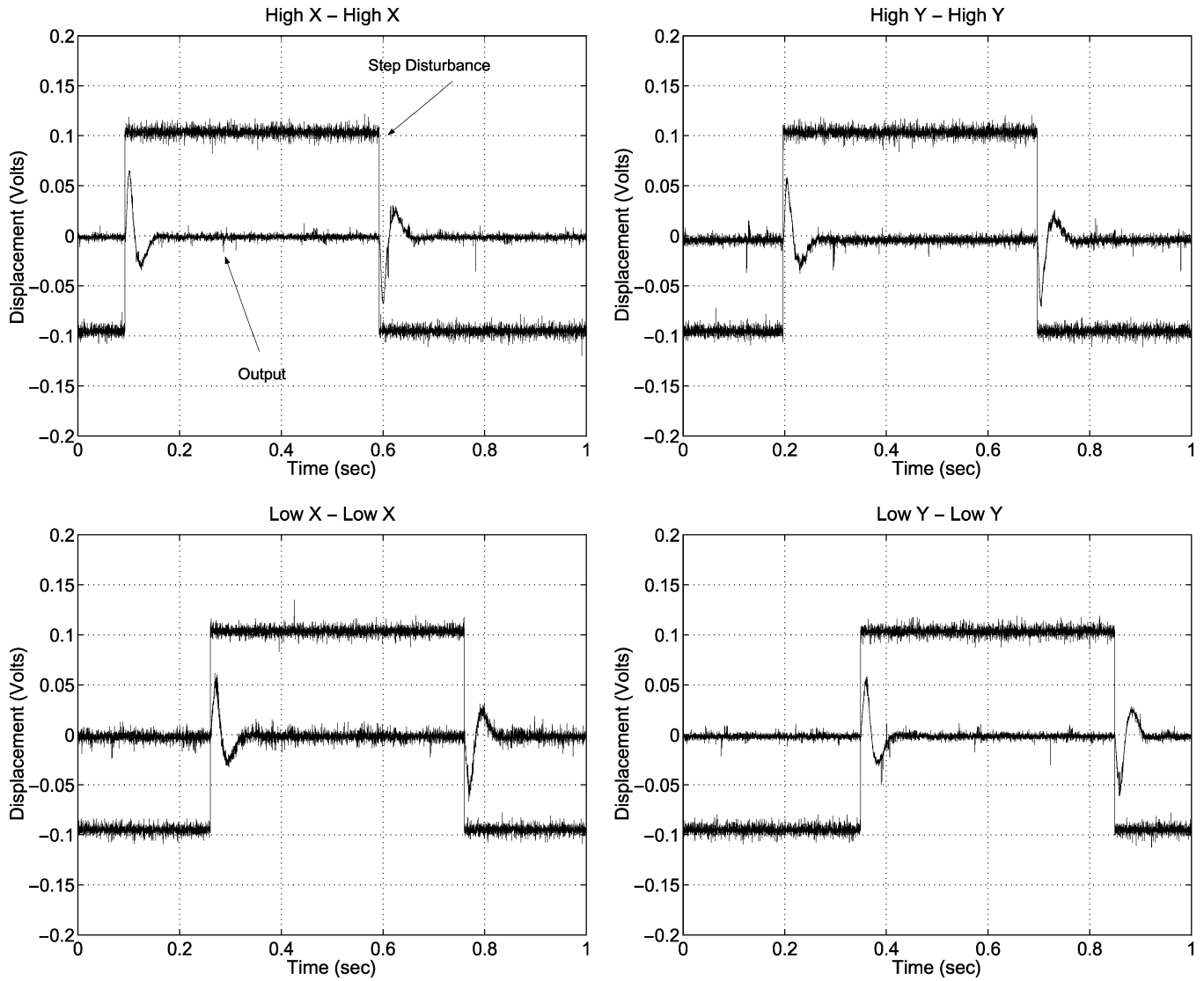

Fig. 13. Disturbance rejection time response from experiments.

bances at the plant input up to a frequency of 10 Hz and beyond a frequency of 200 Hz and that the closed-loop system does not resonate with disturbances in the midfrequency range. All this is also evidenced through the time responses of Fig. 13, where step disturbances are quickly rejected.

The synthesized LTI controller, thus, performed very well in both high-fidelity simulation testing and experiments. Furthermore, the controller achieved a closed-loop bandwidth well above the first three resonant modes of the plant and, hence, experiments confirmed that high-frequency disturbances did not excite these resonant modes of the plant, which could have otherwise been detrimental to stability.

VI. Conclusion

Experience with highly flexible systems shows that unstructured uncertainty does not capture well perturbations on the natural frequencies of the vibrational modes around crossover [24]. This is because the proximity of these lightly damped poles and zeros to the imaginary axis induces large unstructured uncertainties in a gap sense. This is why a simple robust control design with *only* unstructured uncertainties usually fails to perform well on such lightly damped systems when there is significant uncertainty on the natural frequency of the resonant modes. However, unstructured uncertainty is also important when there are significant unmodeled dynamics, as with EMW systems, because of the interaction of the EMW with the substructure or neglected higher order dynamics, for instance. Consequently, a combination of parametric (structured) and unstructured uncertainty has been used in this paper to model the true physical plant. This has led to a new combined application of the well-known $\mathcal{H}_\infty$ loop shaping and μ-synthesis design paradigms for EMW/AMB systems. In addition to capturing the most general form of unstructured uncertainty in the plant (that is, coprime uncertainty) the $\mathcal{H}_\infty$ loop-shaping framework also allows one to directly incorporate performance requirements in terms of the plant loop shape.

The D–K iterative procedure associated with the μ-synthesis leads to high-order controllers that need to be reduced prior to implementation, especially when repeated uncertainty blocks of high dimension are present. In previous works, lower order controllers that are suitable for implementation are obtained through *a posteriori* model reduction. However, performance of the closed-loop system with the reduced order controller is not

easy to ensure using this approach. In this paper, we present a method which alleviates this problem by determining *a priori* the smallest value of the parameter block (which has repeated uncertainty structure), such that guaranteed bounds on the performance degradation of the closed loop can be obtained, in a precise $\mathcal{H}_\infty$ loop-shaping sense.

Finally, the proposed approach when implemented on EMW/AMB gyroscopic systems allows for the incorporation of the parameter-variation due to the rotor speed into the nominal plant (as opposed to treating it totally as unknown uncertainty), thus, leading naturally to a gain-scheduled or parameter-dependent implementation of the synthesized robust controllers.

ACKNOWLEDGMENT

The authors would like to thank Prof. P. Allaire for making available the test rig to experimentally validate the theoretical results of this work and Dr. J. Luo for implementing the controllers on the test rig. They would also like to thank the anonymous reviewers and Associate Editor C. Knospe for their insightful comments.

REFERENCES

[1] A. Lanzon and P. Tsiotras, "Robust control of energy momentum wheels supported on active magnetic bearings using $\mathcal{H}_\infty$ loop-shaping and μ-synthesis," in *Proc. 15th IFAC World Congr.*, Barcelona, Spain, Jul. 2002.

[2] W. W. Anderson and C. R. Keckler, "An integrated power/attitude control system (IPACS) for space application," in *Proc. 5th IFAC Symp. Automatic Control in Space*, 1973.

[3] C. D. Hall, "High-speed flywheels for integrated energy storage and attitude control," in *Proc. Amer. Control Conf.*, Albuquerque, NM, 1997, pp. 1894–1898.

[4] P. Tsiotras, H. Shen, and C. Hall, "Satellite attitude control and power tracking with momentum wheels," *J. Guid. Control Dyn.*, vol. 24, pp. 23–34, 2001.

[5] P. Proctor, "Flywheels show promise for 'high-pulse' satellites," *Aviation Week Space Technol.*, p. 67, Jan. 1999.

[6] B. Shafai, S. Beale, P. LaRocca, and E. Cusson, "Magnetic bearing control systems and adaptive forced balancing," *IEEE Control Syst. Mag.*, vol. 14, no. 2, pp. 4–12, Apr. 1994.

[7] C. R. Knospe, S. M. Tamer, and J. Lindlau, "New results in adaptive vibration control," in *Proc. MAG'97 Industrial Conf. Exhibition on Magnetic Bearings*, Alexandria, VA, Aug. 1997, pp. 209–219.

[8] K. J. Åström and B. Wittenmark, *Adaptive Control*. Reading, MA: Addison-Wesley, 1989.

[9] J. M. Maciejowski, *Multivariable Feedback Design*. Reading, MA: Addison-Wesley, 1994.

[10] M. Green and D. J. N. Limebeer, *Linear Robust Control*. Englewood Cliffs, NJ: Prentice-Hall, 1995.

[11] S. Skogestad and I. Postlethwaite, *Multivariable Feedback Control: Analysis and Design*. New York: Wiley, 1998.

[12] K. Zhou, J. C. Doyle, and K. Glover, *Robust and Optimal Control*. Englewood Cliffs, NJ: Prentice-Hall, 1996.

[13] G. J. Balas and J. C. Doyle, "Robustness and performance tradeoffs in control design for flexible structures," in *Proc. 29th IEEE Conf. Decision and Control*, vol. 6, Honolulu, HI, Dec. 1990, pp. 2999–3010.

[14] J. Luo, P. Tsiotras, S. Djouadi, R. Bartlett, P. Allaire, E. Hilton, and U. Schönhoff, "Flywheel battery magnetic bearing controller design and verification," in *Proc. Space Power Workshop*, Torrance, CA, Apr. 2000.

[15] P. Tsiotras and S. Mason, "Self-scheduled $\mathcal{H}_\infty$ controllers for magnetic bearings," in *Proc. Int. Mechanical Engineering Congr. Exposition*, Atlanta, GA, 1996, pp. 151–158.

[16] S. Sivrioglu and K. Nonami, "LMI approach to gain scheduled $\mathcal{H}_\infty$ control beyond PID control for gyroscopic rotor-magnetic bearing systems," in *Proc. 35th IEEE Conf. Decision and Control*, Kobe, Japan, 1996, pp. 3694–3699.

[17] M. Fujita, K. Hatake, and F. Matsumura, "Loop shaping based robust control of a magnetic bearing," *IEEE Control Syst. Mag.*, vol. 13, no. 4, pp. 57–65, Aug. 1993.

[18] M. Fujita, K. Hatake, F. Matsumura, and K. Uchida, "Experiments on the loop shaping based $\mathcal{H}_\infty$ control of a magnetic bearing," in *Proc. Amer. Control Conf.*, San Francisco, CA, 1993, pp. 8–12.

[19] K. Nonami and T. Ito, "μ-synthesis of flexible rotor-magnetic bearing systems," *IEEE Trans. Contr. Syst. Technol.*, vol. 4, no. 5, pp. 503–512, Sep. 1996.

[20] F. Matsumura, T. Namerikawa, K. Hagiwara, and M. Fujita, "Application of gain scheduled $\mathcal{H}_\infty$ robust controllers to a magnetic bearing," *IEEE Trans. Contr. Syst. Technol.*, vol. 4, no. 5, pp. 484–493, Sep. 1996.

[21] B. A. Francis, *A Course in $\mathcal{H}_\infty$ Control Theory*. New York: Springer-Verlag, 1987, vol. 88.

[22] U. Schönhoff, J. Luo, G. Li, E. Hilton, R. Nordmann, and P. Allaire, "Implementation results of μ-synthesis control for an energy storage flywheel test rig," in *Proc. 7th Int. Symp. Magnetic Bearings*, Zurich, Switzerland, Aug. 2000.

[23] R. Hebner, J. Beno, and A. Walls, "Flywheel batteries come around again," *IEEE Spectrum*, vol. 39, no. 4, pp. 46–51, Apr. 2002.

[24] G. Vinnicombe, *Uncertainty and Feedback: $\mathcal{H}_\infty$ Loop-Shaping and the ν-Gap Metric*. London, U.K.: Imperial College Press, 2000.

[25] G. J. Balas and P. M. Young, "Control design for variations in structural natural frequencies," *J. Guid. Control Dyn.*, vol. 18, no. 2, pp. 325–332, 1995.

[26] A. Packard, "Gain scheduling via linear fractional transformations," *Syst. Control Lett.*, vol. 22, pp. 79–92, 1994.

[27] R. A. Horn and C. R. Johnson, *Matrix Analysis*. Cambridge, U.K.: Cambridge Univ. Press, 1996.

[28] J. C. Doyle, "Structured uncertainty in control systems design," in *Proc. 24th IEEE Conf. Decision and Control*, Ft. Lauderdale, FL, 1985, pp. 260–265.

[29] G. Vinnicombe, "Frequency domain uncertainty and the graph topology," *IEEE Trans. Autom. Control*, vol. 38, no. 9, pp. 1371–1383, Sep. 1993.

[30] D. R. Merkin, *Gyroscopic Systems*. Moscow, U.S.S.R.: Gostekhizdat, 1956.

[31] C. L. Beck, J. Doyle, and K. Glover, "Model reduction of multidimensional and uncertain systems," *IEEE Trans. Autom. Control*, vol. 41, no. 10, pp. 1466–1477, Oct. 1996.

[32] M. K. H. Fan and A. L. Tits, "A measure of worst-case $\mathcal{H}_\infty$ performance and of largest acceptable uncertainty," *Syst. Control Lett.*, vol. 18, no. 6, pp. 409–421, 1992.

[33] J. C. Doyle, B. A. Francis, and A. R. Tannenbaum, *Feedback Control Theory*. New York: MacMillan, 1992.

[34] D. McFarlane and K. Glover, *Robust Controller Design Using Normalized Coprime Factor Plant Descriptions*, 1st ed. New York: Springer-Verlag, 1990, vol. 138.

[35] R. A. Hyde, "$\mathcal{H}_\infty$ aerospace control design—a VSTOL flight application," in *Advances in Industrial Control Series*. New York: Springer-Verlag, 1995.

[36] S. Skogerstad and I. Postlethwaite, *Multivariable Feedback Control*. New York: Wiley, 1996.

[37] D. McFarlane and K. Glover, "A loop shaping design procedure using $\mathcal{H}_\infty$ synthesis," *IEEE Trans. Autom. Control*, vol. 37, no. 6, pp. 759–769, Jun. 1992.

[38] G. Papageorgiou and K. Glover, "$\mathcal{H}_\infty$ loop-shaping: why is it a sensible procedure for designing robust flight controllers?," in *Proc. AIAA Conf. Guidance, Navigation and Control*, Aug. 1999.

[39] K. Glover, G. Vinnicombe, and G. Papageorgiou, "Guaranteed multi-loop stability margins and the gap metric," in *Proc. 39th IEEE Conf. Decision and Control*, Sydney, Australia, Dec. 2000, pp. 4084–4085.

[40] A. Lanzon and R. J. Richards, "A frequency domain optimization algorithm for simultaneous design of performance weights and controllers in μ-synthesis," in *Proc. 38th IEEE Conf. Decision and Control*, vol. 5, Phoenix, AZ, Dec. 1999, pp. 4523–4528.

[41] A. Lanzon and M. W. Cantoni, "A state-space algorithm for the simultaneous optimization of performance weights and controllers in μ-synthesis," in *Proc. 39th IEEE Conf. Decision and Control*, vol. 1, Sydney, Australia, Dec. 2000, pp. 611–616.

[42] ——, "On the formulation and solution of robust performance problems," *Automatica*, vol. 39, no. 10, pp. 1707–1720, Oct. 2003.

[43] P. M. Young, M. P. Newlin, and J. C. Doyle, "Computing bounds for the mixed μ problem," *Int. J. Robust Nonlinear Control*, vol. 5, no. 6, pp. 573–590, Oct. 1995.

[44] P. M. Young and J. C. Doyle, "Properties of the mixed μ problem and its bounds," *IEEE Trans. Autom. Control*, vol. 41, no. 1, pp. 155–159, Jan. 1996.

[45] P. M. Young, "Controller design with real parametric uncertainty," *Int. J. Control*, vol. 65, no. 3, pp. 469–509, Oct. 1996.